# Experimental study of the radiation emitted by 180-GeV/*c* electrons and positrons volume-reflected in a bent crystal

W. Scandale
*CERN, European Organization for Nuclear Research, CH-1211 Geneva 23, Switzerland*

A. Vomiero
*INFM-CNR, Via Vallotti 9, 25133 Brescia, Italy*

S. Baricordi, P. Dalpiaz, M. Fiorini, V. Guidi, and A. Mazzolari
*INFN Sezione di Ferrara and Dipartimento di Fisica, Università di Ferrara, Via Saragat 1, 44100 Ferrara, Italy*

R. Milan
*INFN Laboratori Nazionali di Legnaro, Viale Università 2, 35020 Legnaro (PD), Italy*

G. Della Mea
*Dipartimento di Ingegneria dei Materiali e Tecnologie Industriali, Università di Trento, Via Mesiano 77, 38050 Trento, Italy*

G. Ambrosi, B. Bertucci, W. J. Burger, M. Duranti, and P. Zuccon
*INFN Sezione di Perugia and Dipartimento di Fisica, Università degli Studi di Perugia, Via Pascoli, 06123 Perugia, Italy*

G. Cavoto, F. Iacoangeli, C. Luci, S. Pisano, R. Santacesaria, and P. Valente
*INFN Sezione di Roma, Piazzale Aldo Moro 2, 00185 Roma, Italy*

E. Vallazza
*INFN Sezione di Trieste, Via Valerio 2, 34127 Trieste, Italy*

A. G. Afonin, Yu. A. Chesnokov, V. A. Maisheev, and I. A. Yazynin
*Institute of High Energy Physics, Moscow Region, RU-142284 Protvino, Russia*

A. D. Kovalenko and A. M. Taratin
*Joint Institute for Nuclear Research, Joliot-Curie 6, 141980, Dubna, Moscow Region, Russia*

A. S. Denisov, Yu. A. Gavrikov, Yu. M. Ivanov, L. P. Lapina, L. G. Malyarenko, V. V. Skorobogatov, V. M. Suvarov, and S. A. Vavilov
*Petersburg Nuclear Physics Institute, 188300 Gatchina, Leningrad Region, Russia*

D. Bolognini,* S. Hasan, D. Lietti, A. Mattera, and M. Prest
*Università degli Studi dell'Insubria, Via Valleggio 11, 22100 Como, Italy*
*and INFN Sezione di Milano Bicocca, Piazza della Scienza 3, 20126 Milano, Italy*
(Received 15 September 2008; published 26 January 2009)

The radiation emitted by 180-GeV/*c* volume-reflected electrons and positrons impinging on a bent crystal has been measured by the H8RD22 Collaboration on the H8 beamline at the CERN SPS. A dedicated spectrometer has been developed to measure high-energy photon spectra (up to ~100 GeV) under volume reflection: photon and charged particle beams have been separated by a bending magnet and leptons were detected and tagged by microstrip silicon detectors and a Pb-scintillator sampling calorimeter. A comparison between the experimental and analytical data for the amorphous and volume-reflection cases is presented and the differences are discussed.

DOI: 10.1103/PhysRevA.79.012903 PACS number(s): 61.85.+p, 29.27.−a, 61.80.Fe

## I. INTRODUCTION

After Stark's hypothesis in 1912 [1], in the middle of the 20th century it was shown that the passage of charged particles through straight crystals is characterized by peculiar features in comparison with the passage through amorphous media: the well-known phenomena of channeling [2] and coherent bremsstrahlung of electrons [3] are just two examples. The theoretical explanation of the channeling effect was formulated by Lindhard [4] in 1964; he demonstrated that when a charged particle impinges on a crystal with a

*davide.bolognini@cern.ch

 

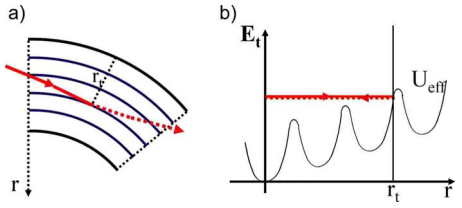


FIG. 1. (Color online) Volume-reflection phenomenon. (a) A charged particle in the crystal volume reflected at the turning radial coordinate $r_t$. (b) The particle transverse energy as a function of the radial coordinate.

small impact parameter with respect to the crystallographic axis (or plane), a number of correlated collisions with the crystal lattice atoms occurs; in the approximation of a small incoming angle the potential of each atom can be replaced with an average continuous potential. In 1976 Tsyganov [5] suggested bending a crystal to steer charged particles: this idea has been developed to obtain high-efficiency extraction of proton and nuclear beams in several experiments on modern accelerators [6–9].

In recent years the volume-reflection (VR) effect has been predicted [10] for positive and negative charged particles and its high efficiency and angular deflection have been experimentally measured [11–13]. The effect takes place in bent crystals when particles with initial incoming angles greater than the channeling angle (that is, with a transverse energy large enough not to be trapped in an atomic planar channel) have a tangency point with respect to the bent planes inside the crystal volume. Figure 1 shows the particle motion and effective potential in a bent crystal in a volume-reflection orientation.

A particle that impinges on the crystal with an angle larger than the critical one ($\theta_c = \sqrt{2U_{\max}/pv}$, where $U_{\max}$ is the maximum value of the potential barrier, $p$ is the particle momentum, and $v$ the velocity) cannot be channeled because of the high transverse momentum: in this case, the angle between the particle and the crystal plane decreases, according to the curvature [Fig. 1(a)]. Considering the noninertial reference system which follows the channel direction [Fig. 1(b)], volume reflection can be described as the reversing of the particle transverse momentum direction at a turning point in the effective potential [10].

While these phenomena are well understood from the theoretical point of view and deeply investigated from the experimental one (for positive particles), radiation emitted by light leptons and volume-reflected in bent crystals is still an open field, given that experiments require stringent beam features and complicated setups. Several papers (see [14] and literature therein) deal with radiation emitted by particles (in particular by electrons and positrons) in the channeling regime; Ref. [14] considers also the coherent bremsstrahlung in bent crystals. However, it is not possible to find in the literature experimental results, apart from [15], which describes the measurement of radiation emitted by positrons in undulatorlike crystals.

This paper presents the results obtained in a test performed at the H8 beamline at the CERN Super Proton Synchrotron (SPS) with 180-GeV/$c$ volume-reflected electrons and positrons; the observation of volume reflection with negative particles obtained in this experiment will be presented separately later [16]. An introduction to the radiation process in bent crystals is described in Sec. II, while Sec. III is devoted to the experimental setup. The spectra obtained are compared with analytical calculations in Sec. IV.

## II. RADIATION FROM BENT CRYSTALS

In a recent paper [17] the radiation by positrons and electrons was considered in the volume-reflection case. The theoretical explanation of this process is based on the analytical description of volume reflection [18] and on the equations derived with the quasiclassical operator method [19], where the probabilities of QED processes may be expressed by classical trajectories of charged particles in electric fields.

The radiation emitted by a relativistic particle can be described [19] with the $\rho$ parameter:

$$\rho = 2\gamma^2\langle v_t^2 - v_m^2\rangle/c^2,$$

where $\gamma$ is the particle Lorentz factor, $\langle v_t^2 - v_m^2\rangle$ is the squared mean deviation of the transverse velocity from its mean value $v_m$, and $c$ is the speed of light. If $\rho \ll 1$, the radiation intensity is the result of interference over a large part of the particle trajectory and depends on the peculiarities of the particle motion. If $\rho \gg 1$, the particle radiates during a small part of the trajectory (its motion direction does not change with the angle $1/\gamma$) and the contributions from far parts can be neglected. The case $\rho \sim 1$ is an intermediate one.

In straight crystals, the first case ($\rho \ll 1$) occurs when the particle planar angle $\theta$ is $\gg \theta_b$, where $\theta_b$ is the characteristic angle defined as $\theta_b = U/mc^2$ ($m$ is the particle mass and $U$ is the planar potential barrier): this type of radiation is known as coherent bremsstrahlung. The opposite case ($\rho \gg 1$) corresponds to synchrotronlike radiation and occurs when $\theta \ll \theta_b$. It is important to note that in a thin crystal a particle conserves the radiation type during its motion.

In a bent crystal, the planar angle $\theta$ changes during the particle motion; if volume reflection occurs, the radiation type during the particle motion is also modified. In other words, far from the reflection point, $\rho \ll 1$ and the radiation is due to coherent bremsstrahlung [14]. Approaching the reflection point, the $\rho$ parameter increases: if the bending radius is significantly greater than the channeling critical one [5], the mean volume reflection angle $\theta_{VR}$ is $\theta_{VR} \approx \sqrt{2}\theta_{ch}$ for positrons and $\theta_{VR} \approx \theta_{ch}$ for electrons [18], where $\theta_{ch} = \sqrt{2U/E}$ is the channeling critical angle ($E$ is the particle energy). Using the expression for $\rho$ for an oscillation near the reflection point, it is possible to estimate $\rho = \gamma\theta_b$ for positrons and $\rho = 0.5\gamma\theta_b$ for electrons. At $\rho = 1$, $E$ corresponds to 12 GeV for positrons and 24 GeV for electrons for the (110) and (111) planes of a single silicon crystal.

Figure 2 shows the behavior of the transverse particle velocity in the area near the reflection point as a function of time: a particle performs an aperiodic oscillation in the transverse plane and the amplitude of the oscillations increases as the particle approaches the reflection point.

The process can be characterized by the $\rho$ parameter, which is calculated over one oscillation period; thus, $\rho$ is a

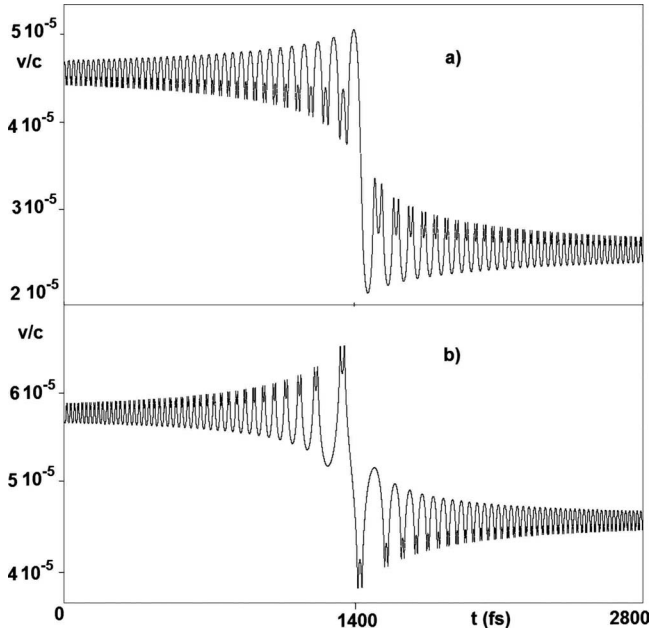


FIG. 2. Relative transverse velocities ($v_t/c$) of 180-GeV/$c$ positrons (a) and electrons (b) at volume reflection in a (111) silicon plane as a function of time (in femtoseconds). The crystal thickness is 0.84 mm, and the bending radius is equal to 12 m for positron and 8 m for electron beams, according to the experimental conditions.

function of the number of periods. According to Fig. 2, the parameter $\rho$ changes from some tenths to some units and, for oscillation at the reflection point, its value is $\approx 30$ for positrons and $\approx 10$ for electrons. It is well known that the periodic planar potential of the (111) plane represents the repetition of the two basic potentials for wide and narrow planes, resulting in different neighboring oscillation amplitudes (Fig. 2).

An estimation of the emitted $\gamma$ energy range is given by the equations [19]

$$\omega = \frac{2\gamma^2\omega_0}{1+\rho/2}, \tag{1}$$

$$E_{\gamma,\max} = \frac{\hbar\omega E}{E+\hbar\omega}, \tag{2}$$

where $\omega_0 = 2\pi/T$ and $T$ is the period of one oscillation set. These relations are written for the radiation first harmonic and for the case of an infinite periodic motion. In other words, Eqs. (1) and (2) define the maximum $\gamma$ energy; the minimum energy is close to zero. Nevertheless, the estimations computed with these relations are in good agreement with calculations (in fact, when $\rho \lesssim 1$ the first harmonic gives the main contribution to the radiation).

Figure 3(a) shows the energy range of the emitted $\gamma$ quanta calculated according to Eqs. (1) and (2): for every oscillation the $\rho$ parameter was found and the corresponding energy was represented in the figure by a vertical line. Figure 3(b) shows the behavior of the intensity and the number of $\gamma$'s as a function of the energy for a simple harmonic motion

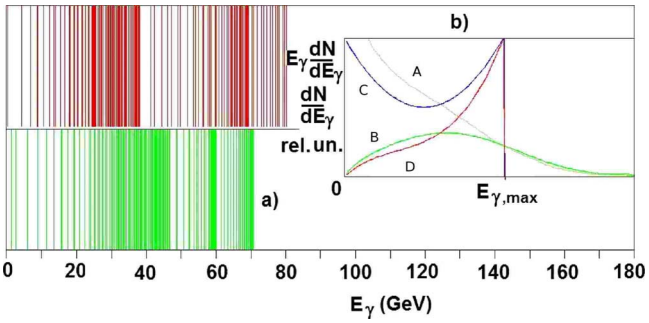


FIG. 3. (Color online) Maximum energies of the $\gamma$ quanta (a) calculated according to Eqs. (1) and (2) from the corresponding frequencies of the motion. Red (top) and green (bottom) lines correspond to 180-GeV/$c$ positrons and electrons, respectively. The shapes (b) of the $\gamma$-quantum spectra and energy losses in periodic structures: the gray ($A$) and green ($B$) curves are the $\gamma$ spectrum and distribution of energy losses for a structure with one period. The blue ($C$) and red ($D$) curves are the same values but for an infinite periodic structure.

in a periodic structure (like an undulator) when this structure has only one oscillation and an infinite number of periods. Even if in the one-period structure the energy could exceed the maximum energy $E_{\gamma,\max}$, it is possible in any case to use Eqs. (1) and (2) to estimate the radiation spectra because the number of emitted $\gamma$ quanta rapidly decreases above $E_{\gamma,\max}$. The greater is $E_{\gamma,\max}$, the smaller is the probability of radiation of the first harmonic as a whole. The relation $I_{\max} = [1+(1+x)^2](1-x)/x$ (from the theory of coherent bremsstrahlung [20]) describes the relative variation of radiation intensity as a function of $x$: in the considered case, $x = E_{\gamma,\max}/E$. This behavior is due to an increase of the longitudinal recoil momentum and hence a decrease of the process formation length.

The expected radiation energy spectrum is peaked approximately at 35 and 45 GeV for positrons and electrons, respectively; the predicted number of $\gamma$'s can be observed up to 70–80 GeV for positrons and up to 70 GeV for electrons due to the influence of the narrow plane. It is clear that the present semiqualitative study is valid for electron (positron) beams (and silicon crystals) in the range of hundreds of GeV: at energies $>1$ TeV the synchrotronlike character of the radiation in a thin crystal should become the dominant one.

Figure 2 presents the behavior of only one possible trajectory for a particle type; as shown in [18] there is a set of trajectories, which have the same incoming angle in a single crystal, but have slightly different transverse energies. At large bending radii, the differences among these trajectories are weak; thus the previous considerations remain valid but in calculations a procedure of averaging has to be taken into account. This procedure smooths the appearance of the small radiation peaks in the case of a single-particle trajectory (see [17]).

From these conditions, it is possible to note that (1) the radiation emitted at volume reflection is intense over a wide angular range of the order of the crystal bending angle; (2) the shape of the radiation spectrum depends on the thickness of the bent crystal: as shown in Fig. 2, this thickness variation is the cause of the energy spread. This is also the reason

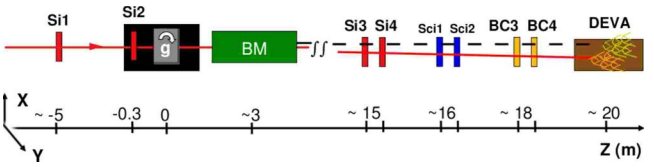


FIG. 4. (Color online) The setup: the microstrip silicon telescope (Si*X*), the high-precision goniometer (g), a bending magnet (BM), the $9.5 \times 9.5$ cm$^2$ silicon beam chambers (BC3, BC4), a pair of scintillators (Sci*X*), and the electromagnetic calorimeter (DEVA).

why the process is usually described in terms of energy loss instead of radiation intensity (which is convenient for straight crystals).

## III. EXPERIMENTAL SETUP

Figure 4 shows the experimental setup on the H8 line of the CERN SPS; it is composed of four modules of a $1.92 \times 1.92$ cm$^2$ double-side silicon telescope (Si*X*) [21], a pair of silicon beam chambers (BC*X*, each made of 2 $9.5 \times 9.5$ cm$^2$ single-side silicon detectors) [22], a high-precision goniometer where a quasimosaic crystal has been positioned [23], a bending magnet (BM), two trigger scintillators (Sci*X*), and an electromagnetic calorimeter (called DEVA).

The incoming particle trajectory (with respect to the crystal orientation) is computed using the spatial information from two 50-$\mu$m readout pitch double-side microstrip silicon telescopes (5-$\mu$m spatial resolution), Si1 and Si2, while the outgoing one is based on the information from Si2 and BC3 (because of multiple scattering, BC4 is used in place of BC3 only in the case of a missing hit on BC3 due to a dead channel). The quasimosaic crystal has been positioned on a high precision goniometer ($\sim$1.5-$\mu$rad angular resolution) which can provide an angular rotation, two independent linear movements, and a cradle for the studies on axial channeling.

The beam particles (which could be light leptons, muons, or light hadrons) are "discriminated" by an electromagnetic lead-scintillator calorimeter (DEVA) that can also be used in the trigger system (together with a pair of scintillators Sci*X*). DEVA (Fig. 5) is formed by 12 2-cm-thick ($15 \times 15$ cm$^2$) scintillator tiles and 11 lead tiles (for a total of $13.07X_0$): the scintillator light is brought out to a 16-channel photomultiplier tube (PMT, H7546, Hamamatsu) by 2-mm-diameter wavelength shifter (WLS) fibers.

The energy spectrum of the whole beam is shown in Fig. 6: the beam is formed by muons (65%), hadrons (12%), and light leptons (23%). In order to collect just the most interesting events, DEVA was part of the trigger, using as a signal the coincidence of the last two scintillator tiles. In the analysis, an event has been identified as a light lepton if its signal overcomes an energy threshold of 10 000 analog-to-digital conversion (ADC) units.

For these preliminary studies on radiation, a $\sim$2-cm-diameter quasimosaic crystal (QM2) and a $2 \times 2$ cm$^2$ one (QM1) have been used (Fig. 7) [23]. The QM2 crystal is 840 $\mu$m thick and has been used with a bending radius of $\sim$12 m; QM1 is 900 $\mu$m thick and has a bending radius of $\sim$8 m. Apart from the radiation studies, the experiment had to analyze the behavior of bent crystals with hadrons; this is the reason for the different bending radii.

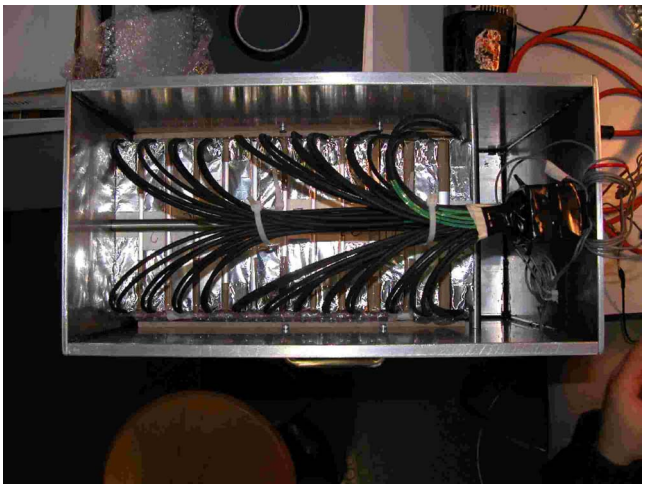

FIG. 5. (Color online) The DEVA calorimeter in the H8 beamline: DEVA is formed by 12 plastic scintillator tiles and 11 lead tiles for a total of $13.07X_0$. The light produced in the scintillators is brought out by WLS fibers to a 16-channel PMT.

## IV. MEASUREMENT RESULTS

In order to improve the analysis that will be described below, geometrical and divergence cuts on the incoming beam have been considered. Geometrical cuts have been implemented mainly to reduce the background events; the

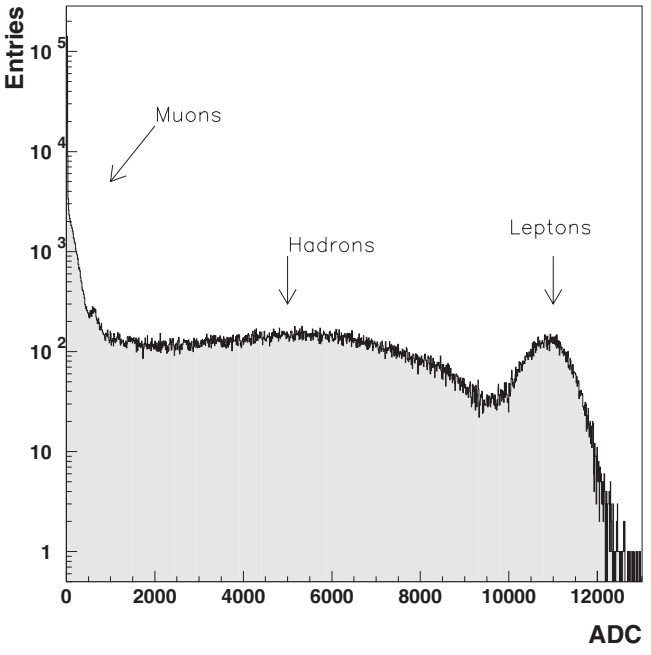


FIG. 6. The H8 beam spectrum measured by the DEVA calorimeter: the first peak corresponds to muons, the central region is populated by hadrons, while the last peak consists of light leptons.

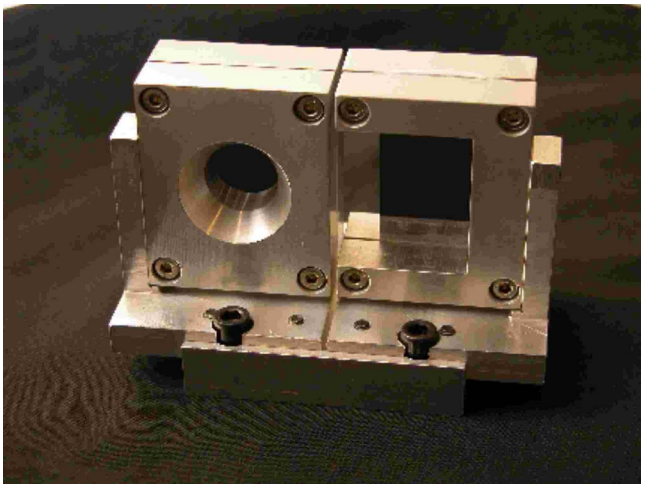

FIG. 7. (Color online) Quasimosaic crystals on their holder. QM2 is the one on the left, QM1 on the right.

beam has a size of ~2.8 mm in horizontal ($X$) and ~2 mm in vertical ($Y$) (rms): for the analysis a range of 4 mm in $X$ and 5 mm in $Y$ has been considered. The incoming beam divergence was measured by the first two silicon detectors to be 25 $\mu$rad in $X$ (Fig. 8) and 46.50 $\mu$rad in $Y$.

The bent crystal is characterized by a critical angle of the order of 15 $\mu$rad at this energy. Thus, in order to select particles with incoming angles smaller than the critical one, a horizontal divergence cut is necessary: $\pm 4$ $\mu$rad is the range chosen for this analysis. In the vertical direction the problem is not so critical, so no divergence cuts have been implemented.

### A. Angular scan

Since the behavior of a bent crystal depends on the particle incoming angle with respect to the crystallographic

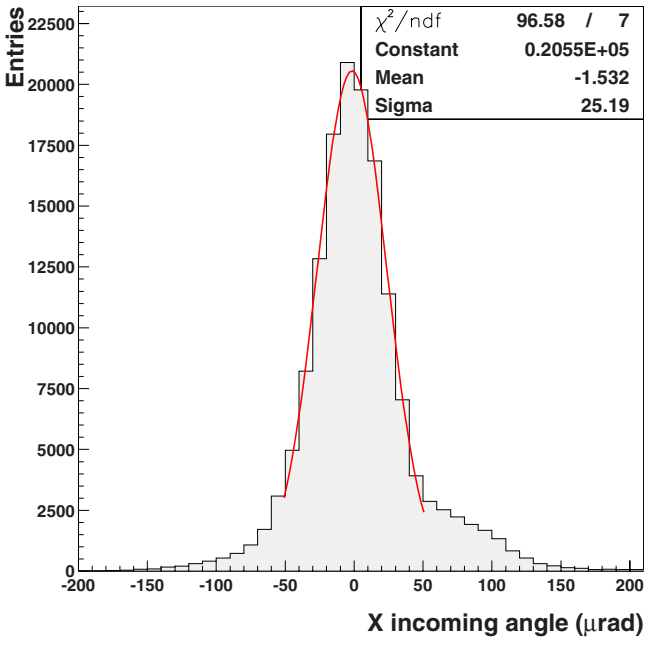


FIG. 8. (Color online) Horizontal incoming angle distribution.

planes, an angular scan has been performed with the following procedure: (1) the crystal is first aligned with respect to the beam by a laser system with a precision of 100 $\mu$rad; (2) a lateral scan is performed in order to evaluate the position of the crystal on the beam; and (3) the angular scan is performed. Figure 9(a) shows an angular scan of the QM2 crystal with 180-GeV/$c$ positrons: the crystal goes from the amorphous condition (up to 4220 $\mu$rad) to the VR effect (from 4240 to 4320 $\mu$rad, with high efficiency and acceptance); then a channeling peak appears (at 4320 $\mu$rad), and finally the crystal goes back to the amorphous state.

For each angular position, a deflection angle distribution is computed: the deflection angle is defined as the difference between the incoming and the outgoing angles; Fig. 9(b) shows the angular distributions at the amorphous (gray) and volume-reflection (white) positions. A Gaussian fit of the amorphous peak provides a rms value of 13.57 $\mu$rad, which is given by the squared sum of the first two detectors, the crystal multiple scattering (most relevant), and the detector resolution (negligible).

The fact that radiation has been emitted can be seen in both plots of Fig. 9: the VR Gaussian left tail in Fig. 9(b) is much higher than the amorphous one.

### B. The spectrometer method

The radiation spectrum can be evaluated by exploiting what can be defined as a spectrometer method, which is schematically shown in Fig. 10. A particle that impinges on the crystal can be in the amorphous, volume-reflection, or channeling state depending on the incoming angle with respect to the crystallographic plane. In all these conditions, the particle can emit photons (yellow dashed line) and lose momentum. In a bending magnet a particle is deflected depending on its momentum, following the equation

$$p\theta = 0.3BL \tag{3}$$

where $p$ is the particle momentum (GeV/$c$), $\theta$ the deflection angle ($\mu$rad), $B$ the magnetic field (T), and $L$ the magnet length (m; in this experiment $BL=1.041$ T m); for unperturbed particles it is possible to define a $\theta_0 = 0.3 \times 1.041/180 = 1735$ $\mu$rad.

Considering Eq. (3), a deflection angle distribution can be translated into an energy loss one: the main peak corresponds to the 180-GeV/$c$ particles, while the tail is due to the particles that have lost energy. Figure 11 shows the energy loss distribution for the VR case.

Finally, the energy spectra $dN/dE$ vs $E$ can be computed: the number of particles in a given bin is divided by the bin width energy value and normalized. The normalization is given by the number of particles in the energy loss distribution ($N$); events with an energy smaller than 0 GeV or greater than 180 GeV are due to the system intrinsic resolution.

The errors on the experimental energy spectrum are given by the uncertainty on the particle numbers in a given bin:

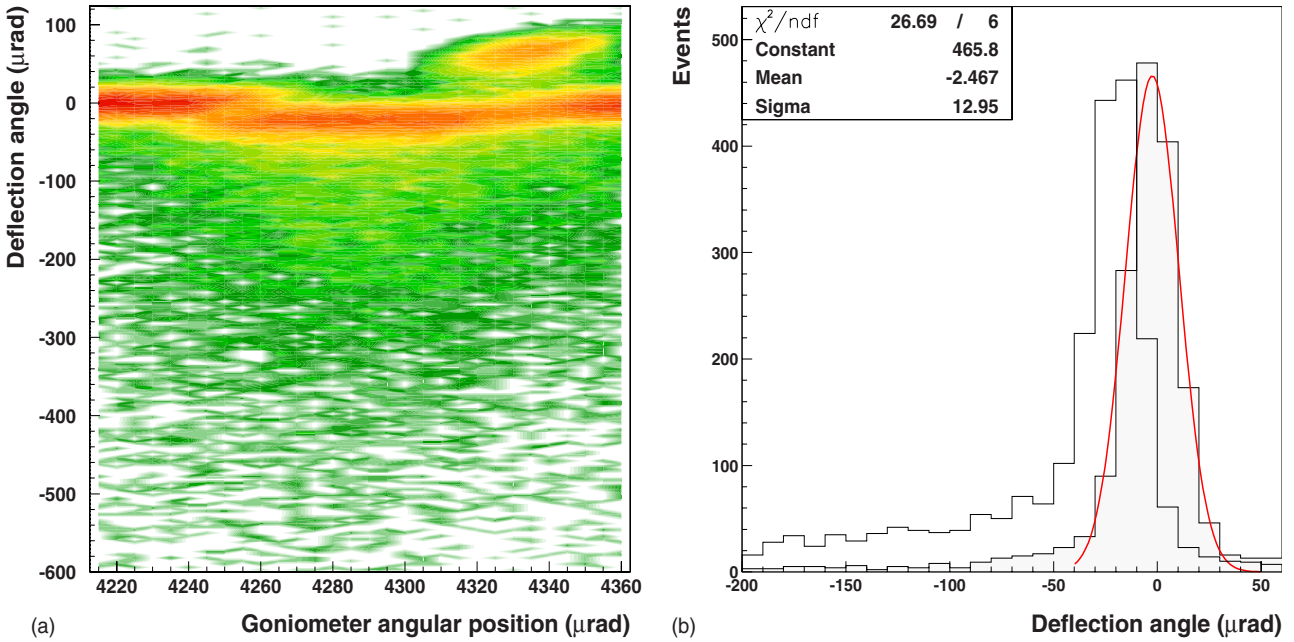


FIG. 9. (Color online) (a) Angular scan: the $x$ axis is the goniometer angle, that is, the crystal angle with respect to the beam, and the $y$ axis is the deflection angle defined as the difference between the incoming and the outgoing angles. (b) The deflection angle distributions in the amorphous (gray) and VR (white) positions: the particles in volume reflection are steered by about 25 $\mu$rad with a high efficiency. The VR Gaussian left tail (which corresponds to the particles that have lost energy) is much higher than the amorphous one.

$$\sigma^2_{dN/dE} = \frac{1}{(N\,dE)^2} dN. \tag{4}$$

As far as the momentum uncertainty is concerned, it is evaluated according to Eq. (3):

$$\sigma^2_{\text{energy loss}} = \left(\frac{0.3BL}{(\theta-\theta_0)^2}\right)^2 \sigma^2_\theta = \frac{(180-p)^4}{(0.3BL)^2}\sigma^2_\theta. \tag{5}$$

$\sigma_\theta$ is the angular error mainly due to the multiple scattering contribution of the material before the bending magnet and is of the order of 15 $\mu$rad.

### C. The amorphous contribution

The amorphous spectrum is given by the bremsstrahlung radiation in the different materials before the bending magnet; a positron that loses energy after the magnet cannot be distinguished from an unperturbed one, so the materials after the magnet must not be taken into consideration. The materials before the bending magnet were (1) two silicon detectors ($2\times300$ $\mu$m); (2) four aluminum sheets in the detector active windows ($4\times20$ $\mu$m); (3) six beam pipe flanges (Mylar) ($6\times180$ $\mu$m); (4) about 3 m of air; and (5) the quasi-mosaic crystal ($\sim$0.09 cm).

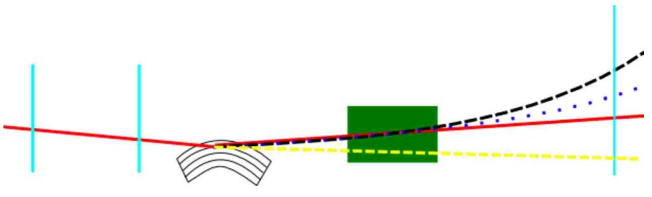

FIG. 10. (Color online) The spectrometer method: a particle in VR can emit photons (yellow dashed line), decreasing its momentum. A bending magnet steers particles depending on their momentum: the solid red line corresponds to a 180-GeV/$c$ particle, while dashed black and dotted blue lines correspond to particles that have lost energy. Silicon detectors (light blue) are able to reconstruct the particle trajectories.

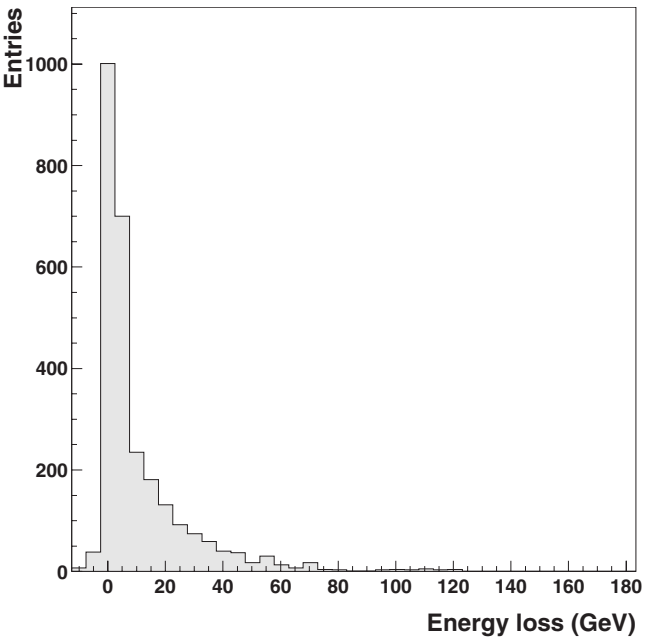


FIG. 11. Energy loss distribution for the volume-reflection case.

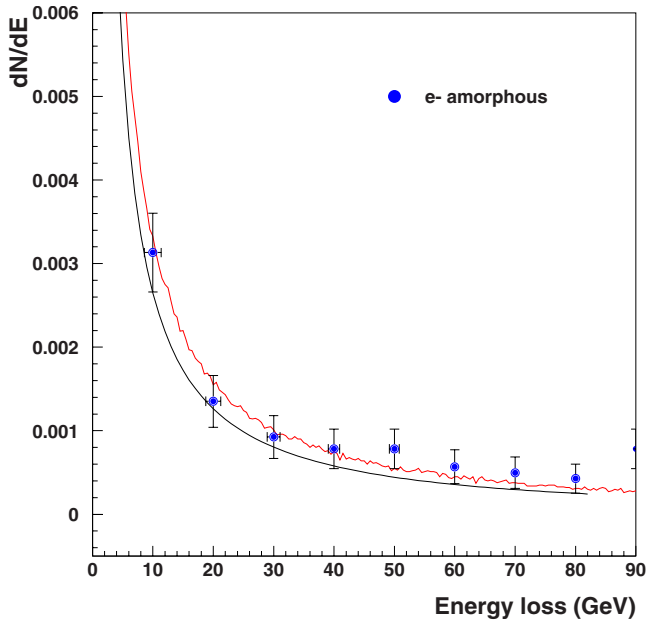


FIG. 12. (Color online) Amorphous spectrum for an electron beam: the figures show a good agreement between experimental data (blue dots) and calculated (black line) and simulated (red line) ones.

The amorphous radiation spectrum has been simulated in two ways: by considering the analytical calculation [17] and by a GEANT3 simulation. The experimental data have been compared with the simulation ones: Fig. 12 shows the comparison between the experimental data (blue dots) and the calculated (black line) and simulated ones (red line) for electrons.

### D. VR radiation spectra

The volume reflection radiation experimental data have been compared with the simulation ones as shown in Fig. 13(a) [Fig. 13(b)] for positrons (electrons). As stated in Sec. II, radiation is usually described in terms of energy loss, that is, as $(dN/dE)E$ vs $E$. Figs. 14(a) [Fig. 14(b)] shows the experimental results (blue dots for amorphous and red or green dots for VR) compared with the calculated ones (black lines) for positrons (electrons).

### E. Discussion

The comparison between the experimental and calculated energy loss spectra shows the following.

(1) There is good agreement between the experimental and calculated energy ranges of emitted $\gamma$-quanta for positrons and electrons with these ranges corresponding to the ones in the semiquantitative analysis of Sec. II (Fig. 2).

(2) The experimental energy losses are smaller than the computed ones by a factor $\approx 1.7$ for positrons and $\approx 1.2$ for electrons.

(3) There is good agreement between experimental and computed spectra for the nonoriented case.

The theoretical calculation method used in this paper has been described in [17] and is based on quasiclassical considerations of QED processes in electric fields [19]. Because of the integration of strongly oscillating functions, the radiation calculation is very complicated and some simplifications of the volume-reflection process have been made. Moreover, in this paper, an averaging procedure over all the particle trajectories has been introduced, in contrast to [17].

Taking into account these considerations, the observed disagreement can be explained as follows.

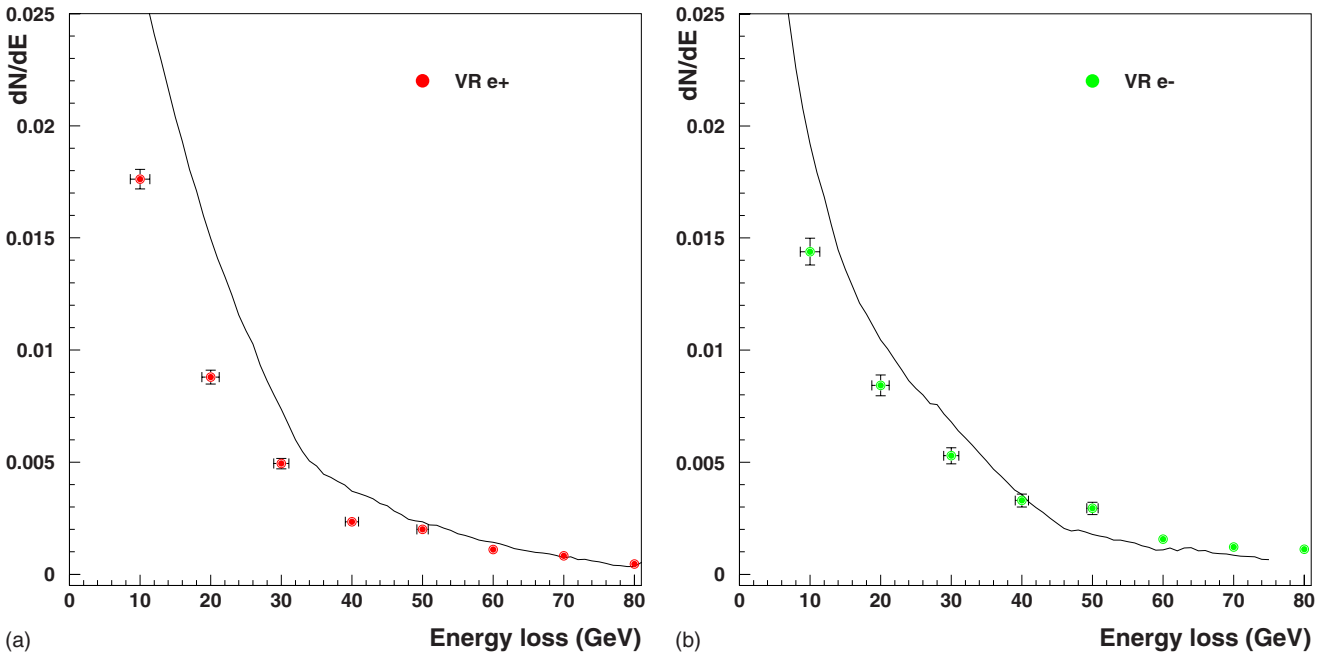


FIG. 13. (Color online) Volume-reflection spectrum for positrons (a) and electrons (b): experimental data (red and green dots) are compared with the calculated ones (black line).

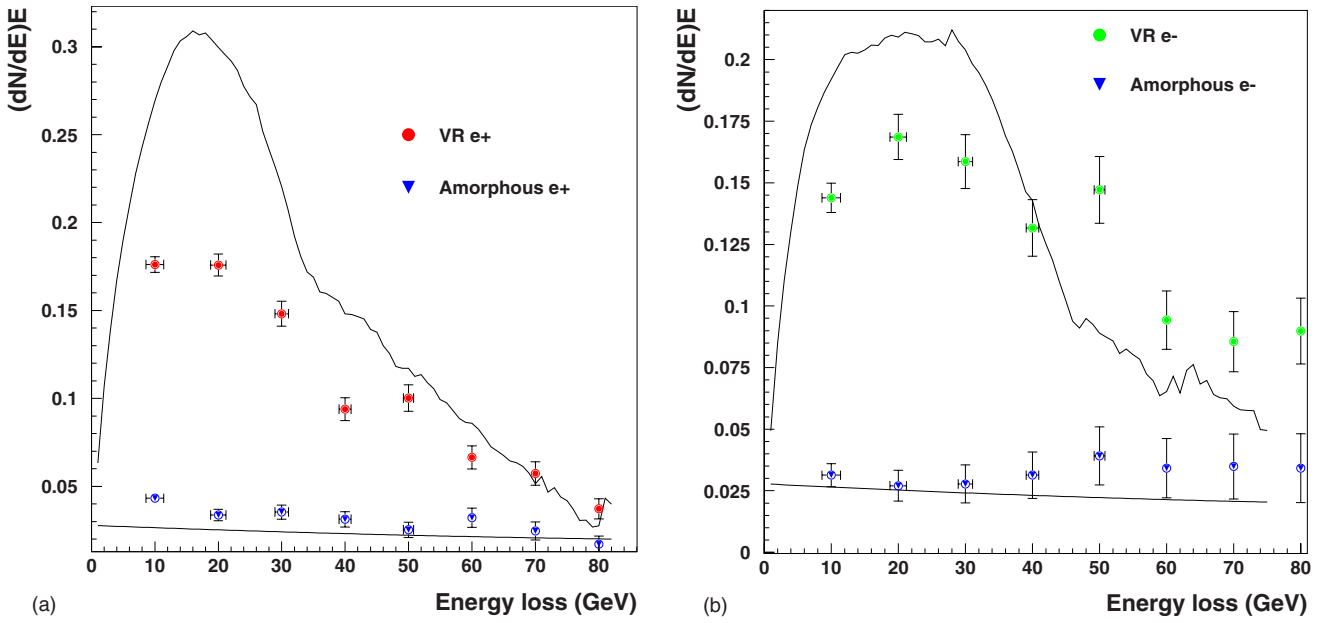


FIG. 14. (Color online) Energy loss spectra $[(dN/dE)E$ vs $E]$ for the positron (a) and electron (b) cases: the blue dots are the experimental amorphous data, the red and green dots represent the volume-reflection experimental results, the black lines identify the volume reflection and amorphous calculated spectra.

(1) The multiple scattering of particles on the crystal atoms has not been considered in the analytical calculations.

(2) The presence of nonhomogeneity of the quasimosaic crystal structure and in particular the dependence of the bending radius on the particle hit position and the torsional effect due to the holder.

(3) A consistent number of particles ($\sim$10–15 %) may be captured in the channeling regime; even if they can exit channeling quickly, the motion changes.

(4) The radiation of two or more $\gamma$ quanta by one particle has not been considered in the calculation.

## V. CONCLUSIONS

Radiation emitted by light particles volume-reflected in bent crystals is still an unexplored field from the experimental point of view. The study presented in this paper has been performed at the CERN SPS H8 line with 180-GeV/$c$ volume-reflected electrons and positrons and a quasimosaic crystal. The radiation spectrum has been measured with a silicon-based spectrometer allowing a resolution better than 1.5 GeV. Experimental data, the analytical calculation and simulation show good agreement for the amorphous case. As far as the spectrum in the VR case is concerned, the energy loss is lower than expected from the calculation; the possible reasons for the disagreement have been considered.

Several applications can be foreseen for radiation emitted by light particles in bent crystals at volume reflection; a very preliminary list could be the following: (1) the generation of intense $\gamma$ beams for a positron source [24]; (2) the generation of positron beams and the collimation of electron-positron beams at a future linear collider [25]; and (3) the generation of intense $\gamma$ beams for medical applications. New tests are foreseen by the Collaboration with an improved experimental setup (calorimeters to tag electrons and to measure the photon spectrum, reduction of the multiple scattering due to air, selection of a dedicated crystal) at low and high energy in the near future.

## ACKNOWLEDGMENTS

The tracking detectors have been provided by Professor L. Lanceri (INFN and University of Trieste). The work has been partially supported by the Italian Research and University Ministry (Research Project No. PRIN06). This work was partly supported by the Russian Foundation for Basic Research (Grant No. 06-02-16912), the "Elementary Particle Physics and Fundamental Nuclear Physics" Program of Russian Academy of Sciences, the INFN-NTA-HCCC program, the INTAS-CERN Foundation (Grant No. 05-103-7525), and the MIUR Project No. 2006028442.

[1] J. Stark, Phys. Z. **12**, 973 (1912).
[2] D. S. Gemmell, Rev. Mod. Phys. **46**, 129 (1974).
[3] M. L. Ter-Mikaelian, *High Energy Electromagnetic Processes in Condensed Media* (Wiley, New York, 1972).
[4] J. Lindhard, Phys. Lett. **12**, 126128 (1964).
[5] E. N. Tsyganov, Fermilab Report No. TM-682, 1976 (unpublished); Fermilab Report No. TM-684, 1976 (unpublished).
[6] A. G. Afonin *et al.*, JETP **74**, 55 (2001).

[7] H. Akbari *et al.*, Phys. Lett. B **313**, 491 (1993).
[8] R. A. Carrigan, Jr., *et al.*, Nucl. Instrum. Methods Phys. Res. B **90**, 128 (1994).
[9] A. Baurichter *et al.*, Nucl. Instrum. Methods Phys. Res. B **164–165**, 27 (2000).
[10] A. M. Taratin and S. A. Vorobiev, Phys. Lett. A **119**, 425 (1987).
[11] Y. M. Ivanov *et al.*, Phys. Rev. Lett. **97**, 144801 (2006).
[12] Y. M. Ivanov *et al.*, JETP Lett. **84**, 372 (2006).
[13] W. Scandale *et al.*, Phys. Rev. Lett. **98**, 154801 (2007).
[14] V. A. Arutyunov *et al.*, Nucl. Phys. B **363**, 283 (1991).
[15] V. T. Baranov *et al.*, Nucl. Instrum. Methods Phys. Res. B **252**, 32 (2006).
[16] W. Scandale *et al.* (unpublished).
[17] Yu. A. Chesnokov *et al.*, JINST **3**, P02005 (2008).
[18] V. A. Maisheev, Phys. Rev. ST Accel. Beams **10**, 084701 (2007).
[19] V. N. Baier, V. M. Katkov, and V. M. Strakhovenko, *Electromagnetic Processes at High Energies in Oriented Single Crystals* (Word Scientific, Singapore, 1998).
[20] H. Bilokon *et al.*, Nucl. Instrum. Methods Phys. Res. **204**, 299 (1983).
[21] L. Celano *et al.*, Nucl. Instrum. Methods Phys. Res. A **381**, 49 (1996).
[22] M. Prest *et al.*, Nucl. Instrum. Methods Phys. Res. A **501**, 280 (2003).
[23] W. Scandale *et al.*, Rev. Sci. Instrum. **79**, 023303 (2008).
[24] T. Suwada *et al.*, Phys. Rev. ST Accel. Beams **10**, 073501 (2007).
[25] A. Seryi *et al.*, in Proceedings of the Particle Accelerator Conference (PAC 07), Albuquerque, New Mexico, 2007 (unpublished).